J Geod (2014) 88:901–914
DOI 10.1007/s00190-014-0730-z

ORIGINAL ARTICLE

A fixed full-matrix method for determining ice sheet height change from satellite altimeter: an ENVISAT case study in East Antarctica with backscatter analysis

Yuande Yang · Cheinway Hwang · Dongchen E

Received: 17 September 2013 / Accepted: 15 May 2014 / Published online: 4 June 2014

Abstract A new method, called the fixed full-matrix method (FFM), is used to compute height changes at crossovers of satellite altimeter ground tracks. Using the ENVISAT data in East Antarctica, FFM results in crossovers of altimeter heights that are 1.9 and 79 times more than those from the fixed half method (FHM) and the one-row method (ORM). The mean standard error of height changes is about 14 cm from ORM, which is reduced to 7 cm by FHM and to 3 cm by FFM. Unlike FHM, FFM leads to uniform errors in the first-half and second-half height-change time series. FFM has the advantage in improving the accuracy of the change of height and backscattered power over ORM and FHM. Assisted by the ICESat-derived height changes, we determine the optimal threshold correlation coefficient (TCC) for a best correction for the backscatter effect on ENVISAT height changes. The TCC value of 0.92 yields an optimal result for FFM. With this value, FFM yields ENVISAT-derived height change rates in East Antarctica mostly falling between −3 and 3 cm/year, and matching the ICESat result to 0.94 cm/year. The ENVISAT result will provide a constraint on the current mass balance result along the Chinese expedition route CHINARE.

Keywords Altimeter · Backscatter · East Antarctica · ENVISAT · Fixed full-matrix method

1 Introduction

With an area of 15 million km^2 and an average ice thickness of 2 km, the Antarctic ice sheet holds about 90 % of the Earth's ice. Melting of the ice here will contribute significantly to sea level rise (Church et al. 2001). In the extreme case, a complete meltdown of the Antarctic ice sheet will increase sea level by 60 m. Several phenomena are associated with ice melting over the Antarctic ice sheet. One such phenomenon is ice height changes, but a large-scale measurement of such changes here will be difficult without using remote sensing satellites. A satellite altimeter can provide with direct measurements of height changes over ice sheets, as demonstrated by, among others, Zwally et al. (1989), Zwally and Brenner (2001), Davis and Ferguson (2004) and Wingham et al. (2006).

A satellite altimeter repeats its ground tracks at a designated time interval called repeat period. For example, the repeat periods of the Geosat/ERM, ENVISAT and TOPEX/Poseidon altimeters are 17, 35 and 10 days, respectively. A complete list of the repeat periods for all altimeter missions can be found at the AVISO web site (http://www.aviso.oceanobs.com/en/missions.html), and in Fu and Cazenave (2001) for earlier altimeter missions. Given repeat measurements over the same spot, a height-change time series can be constructed. A typical component of a height-change time series over an ice sheet is the seasonal variation (Davis and Segura 2001), which is largely caused by seasonal

Y. Yang · D. E
Chinese Antarctic Center of Surveying and Mapping, Wuhan University, 129 Luoyu Road, Wuhan 430079, China

C. Hwang (✉)
Department of Civil Engineering, National Chiao Tung University, 1001 Ta Hsueh Road, Hsinchu, Taiwan, ROC
e-mail: Cheinway@mail.nctu.edu.tw; cheinway@gmail.com
URL: http://space.cv.nctu.edu.tw

C. Hwang
School of Geodesy and Geomatics, Wuhan University, 129 Luoyu Road, Wuhan 430079, China

snow accumulation and melting. A sufficiently long record (say 10 years) of ice sheet height change may reveal signals about climate change and be used to infer the long-term contribution of ice sheet melting to sea level rise. Assisted by gravity observations from missions such as GRACE (Tapley et al. 2004), height changes from satellite altimeters can reveal the mass balance over the Antarctic (Wahr et al. 2000; Velicogna and Wahr 2006).

At a given spot or a "bin" (a bin is defined by a rectangular box bordered by two lines of latitude and longitude), several methods can be used to derive height changes from repeat altimeter measurements. Two popular methods are currently in use: one uses altimeter measurements at crossover points (the crossover method) and the other along-track repeat measurements (the along-track method). The crossover method has the advantages over the along-track method in reducing the geographic correlated error and the antenna polarization error (Rémy and Parouty 2009). Earlier crossover methods, such as that used by Yi et al. (1997), determined ice sheet height changes with respect to a single reference month, resulting in only a small amount of altimeter-derived observations. The method of Yi et al. (1997) is called one-row method (ORM) and was improved by Zwally and Brenner (2001), Ferguson et al. (2004) and Li and Davis (2006) later. In the fixed half-matrix method (FHM), Zwally and Brenner (2001) and Ferguson et al. (2004) used a globally fixed reference month when generating improved height changes to form an upper triangular matrix. Notice that the main difference between Zwally and Brenner (2001) and Ferguson et al. (2004) lies in the different ways of using weights for height changes from altimeters. In the dynamic upper triangular matrix method (DHM), Li and Davis (2006) dynamically selected the reference month to maximize the crossover number of altimeter-derived height changes for any given bin.

Because of the importance of Antarctica ice sheet height changes and the motivation to optimize the altimeter determination of such changes, the objective of this paper is to demonstrate an improved method for constructing height-change time series and to demonstrate the backscatter effect on the altimeter-derived height changes. We will use the crossover method to construct height changes in this paper. Like the method of Ferguson et al. (2004), our method will use a globally fixed reference month. However, for improvement we will introduce a lower triangular matrix to form a full matrix that dramatically increases the number of crossover observations and reduces errors in height changes. As such, our method is called the fixed full-matrix method (FFM). With FFM and other existing methods, we will use ENVISAT altimeter data to determine height-change time series in a region over the Antarctic ice sheet. This region is in East Antarctica and is bordered by longitudes from 60° to 80°E, and latitudes from 65° to 81.6°S. Changes in the ice sheet heights here constitute an important part of mass balance

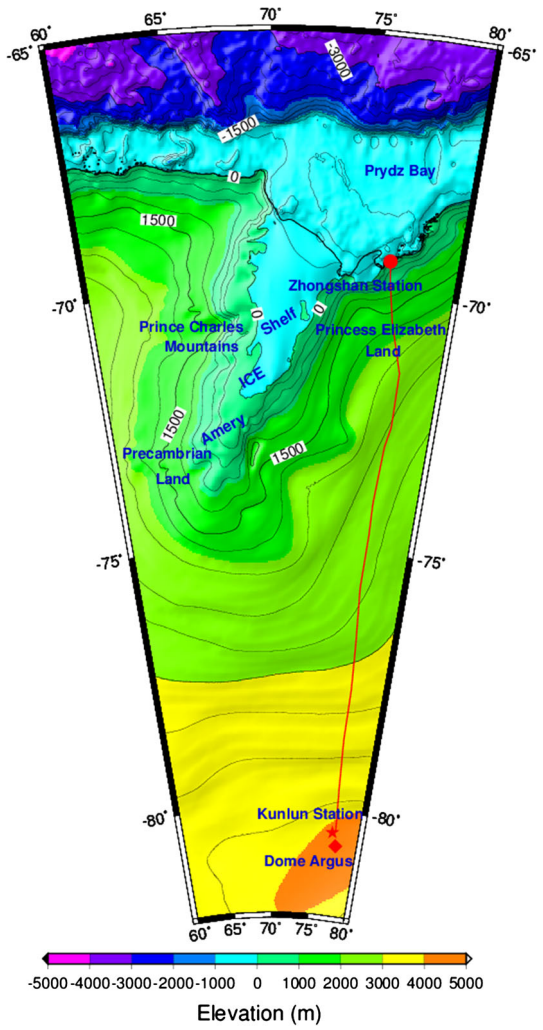

Fig. 1 Topography of East Antarctica with major surface features and the CHINARE expedition route from Zhongshan Station (*solid circle*) to Dome Argus (*diamond*) and Kunlun Station (*star*)

study in the Antarctica. In addition, this study area covers the expedition route of the Chinese National Antarctic Research Expedition (CHINARE) in the 1996–1997 austral summers. This route started from Zhongshan Station, via Dome Argus (called Dome A for short) and finished at Kunlun Station (Fig. 1) close to the South Pole. Since the 1996–1997 expedition, campaign-mode GPS observations at a 1-year interval have been collected along this route and were used to estimate horizontal velocities of ice sheet and mass balances along this route (Zhang et al. 2008; Ding et al. 2011). However, there was no estimate of height change from such GPS data. The height changes from the ENVISAT altimeter data in this paper can be used to estimate height changes along this route and to assess the pattern of ice sheet variation here. The ENVISAT result will provide critical information for planning future GPS campaigns in the region.

2 The fixed full-matrix method for determining ice sheet height change from altimeter

2.1 The theory of the fixed full-matrix method

Here, we present the theory of FFM for determining a time series of height changes at a given bin (a bin is defined in Sect. 1). The notations below follow those used in Zwally and Brenner (2001), Davis and Segura (2001), Ferguson et al. (2004) and Li and Davis (2006). An altimeter-observed height difference, ΔH, at the crossover of two crossing ground tracks can be expressed as (here we show the case of an ascending track and a descending track)

$$\Delta H = \begin{cases} \Delta H_R + B_{\mathrm{A}} - B_{\mathrm{D}} + \Delta H_{\mathrm{S}} & t_{\mathrm{A}} > t_{\mathrm{D}} \\ \Delta H_R + B_{\mathrm{D}} - B_{\mathrm{A}} + \Delta H_{\mathrm{S}} & t_{\mathrm{D}} > t_{\mathrm{A}} \end{cases} \tag{1}$$

where t_{A} and t_{D} are the times associated with ascending track and descending track, ΔH_R the true height change, B_{A} and B_{D} the time-independent biases resulting from directional dependencies in the orbit error, ΔH_{S} is the spurious ice sheet surface height change, mainly induced by backscattered power change.

Because the heights from the ascending and descending tracks are measured at the same location, the slope effects on both heights are common and will be largely canceled upon differencing, especially when the difference between the altitudes of the ascending and descending orbits is small. It is clear ΔH in Eq. (1) is the height difference in the time interval of $|t_{\mathrm{A}} - t_{\mathrm{D}}|$. For a given month j, the height difference with respect to the height in a reference month for $i\,(j \geq i)$ can be computed. Such a height difference can be formed from an ascending and a descending track (the AD case) or a descending and an ascending track (the DA case). For a given bin, there can be many crossovers. The average height difference at a bin is computed by combining the mean of all AD height differences, $\overline{\Delta H}_{\mathrm{AD}}$, and the mean of all DA height differences, $\overline{\Delta H}_{\mathrm{DA}}$ (Zwally et al. 1989; Ferguson et al. 2004):

$$\overline{\Delta H}_{i,j} = \omega_{\mathrm{AD}} \cdot \overline{\Delta H}_{\mathrm{AD}} + (1 - \omega_{\mathrm{AD}}) \cdot \overline{\Delta H}_{\mathrm{DA}} \tag{2}$$

where $\omega_{\mathrm{AD}} = n_{\mathrm{AD}}/(n_{\mathrm{AD}} + n_{\mathrm{DA}})$, with n_{AD} and n_{DA} being respectively the numbers of crossovers formed by AD and DA tracks in 1 month, and the total number of crossovers is $n_{i,j} = n_{\mathrm{AD}} + n_{\mathrm{DA}}$. The standard error of $\overline{\Delta H}_{i,j}$ is computed as

$$\sigma_{i,j} = \sqrt{\omega_{\mathrm{AD}}^2 \cdot \sigma_{\mathrm{AD}}^2 + (1 - \omega_{\mathrm{AD}})^2 \cdot \sigma_{\mathrm{DA}}^2} \tag{3}$$

where σ_{AD} and σ_{DA} are the standard errors of $\overline{\Delta H}_{\mathrm{AD}}$ and $\overline{\Delta H}_{\mathrm{DA}}$, respectively. If n_{AD} and n_{DA} are sufficiently large, B_{A} and B_{D} can be reduced or even eliminated (Ferguson et al. 2004). Ignoring B_{A} and B_{D} in Eq. (1) and considering the months (i, j) leads to

$$\overline{\Delta H}_{i,j} = \overline{\Delta H}_{R(i,j)} + \overline{\Delta H}_{S(i,j)}(t) \tag{4}$$

where $\overline{\Delta H}_{R(i,j)}$ and $\overline{\Delta H}_{S(i,j)}(t)$ are the mean height change and the error due to backscatter, respectively. We will name the term $\overline{\Delta H}_{S(i,j)}(t)$ backscatter correction below (Zwally and Brenner 2001).

For a given bin with N months of altimeter observations, we can form an upper triangular matrix of mean height changes as follows

$$\overline{\Delta \mathbf{H}} = \begin{bmatrix} \overline{\Delta H}_{1,1} & \overline{\Delta H}_{1,2} & \overline{\Delta H}_{1,3} & \cdots & \overline{\Delta H}_{1,N} \\ - & \overline{\Delta H}_{2,2} & \overline{\Delta H}_{2,3} & \cdots & \overline{\Delta H}_{2,N} \\ - & - & \cdots & \cdots & \cdots \\ - & - & - & \cdots & \overline{\Delta H}_{(N-1),N} \\ - & - & - & - & \overline{\Delta H}_{N,N} \end{bmatrix} \tag{5}$$

where the elements with the sign "–" are ignored by definition. A matrix element $\overline{\Delta H}_{i,j}$ represents the mean height change between month i and month j, computed by Eq. (2).

In the ORM method, only the height changes in the first row, i.e., $\overline{\Delta H}_{1,j}$, $j = 2, \ldots, N$, are used to form a time series for height-change rate (e.g., Yi et al. 1997). However, Zwally and Brenner (2001, Eqs. (17)–(18)) and Ferguson et al. (2004, Eq. (5)) show that, in addition to the elements in the first row, other elements of $\overline{\Delta \mathbf{H}}$ can be used to construct an improved time series of height change. Use of modified elements in the upper triangular part of $\overline{\Delta \mathbf{H}}$ leads to the FHM method. In fact, there are two different computational algorithms in the FHM method. In the first algorithm, the following recursive formula is used to form a time series of height change, H_j, using the elements in Eq. (5)

$$H_j = \frac{1}{j-1}\left[\overline{\Delta H}_{1,j} + \sum_{i=2}^{j-1}(H_i + \overline{\Delta H}_{i,j})\right], \quad j = 3, \ldots, N \tag{6}$$

with the starting values $H_1 = \overline{\Delta H}_{1,1} = 0$ and $H_2 = \overline{\Delta H}_{1,2}$. Note that Eq. (6) here is a compact representation of the two recursive equations of Zwally and Brenner (2001, Eqs. (17)–(18)). The notation H_j in Eq. (6) is the height change of month j with respect to month one, which is the mean value of the direct height change $\overline{\Delta H}_{1,j}$ and the indirect (inferred) height changes $\overline{\Delta H}_{i,j}$ shifted by H_i (each shift makes an indirect height change referring to month one).

In the second algorithm, the indirect height changes $\overline{\Delta H}_{i,j}$ are first shifted by the elements in the first row $\overline{\Delta H}_{1,i}$ as

$$\overline{\Delta H'}_{i,j} = \overline{\Delta H}_{1,i} + \overline{\Delta H}_{i,j}, \quad \text{for } j > i > 1 \tag{7}$$

where $\overline{\Delta H'}_{i,j}$ is now the indirect height change of month j with respect to month one, as contributed by the shifted $\overline{\Delta H}_{i,j}$. The second algorithm was used by Ferguson et al. (2004, Eq. (5)). Like Eq. (6), the mean height change of

month j with respect to month one can be computed from the direct and indirect height changes as

$$H_j = \frac{1}{j-1}\left(\overline{\Delta H}_{1,j} + \sum_{i=2}^{j-1} \overline{\Delta H'}_{i,j}\right), \quad j = 3, \ldots, N \quad (8)$$

In Eq. (6), the weights for $\overline{\Delta H}_{1,j}$ and $\overline{\Delta H'}_{i,j}$ are identically $1/(j-1)$. In both the first and second algorithms, the number of height changes used to form H_j increases with j, so the standard error of H_j will decrease with j (because more measurements are used for a larger j). Furthermore, if we replace $1/(j-1)$ by a weight based on the number of crossovers, Eq. (8) becomes

$$H_j = w_{1,j}\overline{\Delta H}_{1,j} + \sum_{i=2}^{j-1} w_{i,j}\overline{\Delta H'}_{i,j}, \quad j = 3, \ldots, N \quad (9)$$

where $w_{i,j} (i = 1, \ldots, j-1)$ is the ratio between the number of crossovers for $\overline{\Delta H}_{i,j}$ and the total number of crossovers for all the contributing height changes in Eq. (9).

In the two algorithms for FHM, the authors (e.g., Zwally and Brenner 2001; Ferguson et al. 2004) have used heights at crossovers to form forward height changes. As seen in Eq. (5), one height can be used to form multiple height changes, which are not totally independent. A height change in Eq. (5) is like the phase difference at a pixel of an interferogram formed by two SAR images, and one SAR image can be used to form multiple interferograms, which are not fully independent. For example, if there are 10 SAR images, up to 45 possible pairs can be formed and used, but only 9 pairs are independent [these are like the elements of the first row in the matrix of Eq. (5)].

Based on the second algorithm of FHM, we extend the use of height changes in Eq. (5) as follows. The key is to fill the undefined height changes [with shifts of height changes as in Eq. (7)] in the lower triangular part of $\overline{\Delta \mathbf{H}}$ in Eq. (5). Following the principle in Eq. (7), we can form backward shifted height changes as

$$\overline{\Delta H'}_{i,j} = \overline{\Delta H}_{1,i} - \overline{\Delta H}_{j,i}, \quad \text{for } i > j \geq 2 \quad (10)$$

where $\overline{\Delta H'}_{i,j}$ is now the indirect (inferred) height change of month j with respect to month one. One must be cautious about the different elements that are used to form the shifted height changes (with respect to month one) in Eqs. (7) and (10) for the upper and lower triangular parts. With $\overline{\Delta H'}_{i,j}$ from Eqs. (7) and (10), we can form a full matrix of shifted height changes relative to month one as

$$\overline{\Delta \mathbf{H}'} = (\overline{\Delta H'}_{i,j}) \quad (11)$$

where the symbol in the brackets on the right-hand side represents the matrix elements, as in a standard matrix treatise. Note that the diagonal elements in $\overline{\Delta \mathbf{H}'}$ are undefined, except for the first one, e.g., $\overline{\Delta H'}_{1,1} = 0$. A row vector of $\overline{\Delta \mathbf{H}'}$ contains the height differences from month 2 to N (with respect to month one; except the diagonal elements), and there are $(N-1)$ such row vectors that can be used to compute the mean height change for a particular month. Because FHM [see Eq. (8)] can use the height changes in the upper triangular matrix of $\overline{\Delta \mathbf{H}'}$, naturally the method can also use the height changes in the lower triangular matrix of $\overline{\Delta \mathbf{H}'}$. That is, the logic of using the lower triangular elements of the full matrix [Eq. (11)] follows exactly the same logic used for FHM [however, different height shifts are used for the upper and lower elements, see Eqs. (7) and (10)]. In summary, FFM uses the concept of FHM, but extends to use also the lower triangular elements to produce a time series of uniform precision (see Fig. 4 below for uniform precision). When using the lower triangular part, the mean height change of month j with respect to month one is computed as

$$H_j = \frac{1}{N-j}\sum_{i=j+1}^{N} \overline{\Delta \mathbf{H}'}_{i,j}, \quad j = 2, \ldots, N-1 \quad (12)$$

which is similar to Eq. (8), but based on the shifted height changes in the lower triangular part of $\overline{\Delta \mathbf{H}'}$. By definition, $H_1 = 0$ (height change of the first month is zero) and H_N is undefined. Therefore, one can choose to use shifted height changes from either the upper triangular or the lower triangular part of $\overline{\Delta \mathbf{H}'}$ for FHM. However, the resulting height precisions will have different patterns: as j goes from 2 to N, use of the upper triangular part of $\overline{\Delta \mathbf{H}'}$ will lead to progressively improved height precisions [j increasing in Eq. (8)], while use of the lower triangular part will lead to progressively degraded height precisions [$(N-j)$ decreasing in Eq. (12)].

Because of the non-uniform height precision nature of FHM, an improved strategy will be one that uses all height changes in $\overline{\Delta \mathbf{H}'}$ to achieve a uniform height precision. In light of this, we propose the fixed full-matrix method (FFM) that uses all elements of $\overline{\Delta \mathbf{H}'}$ (except the diagonal elements). Here, "fixed" means "tied" to the first month, i.e., all height changes are relative to month one. The weighted average of height changes from FHM and lower triangular finally formed the height change of FFM. By FFM, the mean height change of month j relative to month one is computed from the $(N-1)$ height changes as

$$H_j = \frac{1}{N-1}\sum_{i=1, i\neq j}^{N} \overline{\Delta \mathbf{H}'}_{i,j} \quad j = 2, \ldots, N \quad (13)$$

Furthermore, one can replace the weight $1/(N-1)$ in Eq. (13) by a weight based on the number of crossovers. This leads to the final formula for computing a time series of height

change by FFM in this paper:

$$\overline{H}_j = \sum_{i=1, i\neq j}^{N} \omega_{i,j} \cdot \overline{\Delta \mathbf{H}'}_{i,j}, \quad j = 2, \ldots, N \tag{14}$$

By error propagation, the standard error of $\overline{H}_j$ is

$$\bar{\sigma}_j = \sqrt{\sum_{i=1, i\neq j}^{N} (\omega_{i,j} \cdot \sigma'_{i,j})^2}, \quad j = 2, \ldots, N \tag{15}$$

where $\omega_{i,j} = n'_{i,j}/n_j$ with $n'_{i,j}$ being the number of crossovers used to compute $\overline{\Delta H'}_{i,j}$, $n_j = \sum_{i=1, i\neq j}^{N} n'_{i,j}$, and

$$\sigma'_{i,j} = \begin{cases} \sigma^2_{1,j}, & \text{for } i = 1 \\ \sqrt{\sigma^2_{1,i} + \sigma^2_{i,j}}, & \text{for } j > i > 1 \\ \sqrt{\sigma^2_{1,i} + \sigma^2_{j,i}}, & \text{for } i > j \geq 2 \end{cases} \tag{16}$$

We can expect that, compared to ORM and FHM, FFM can substantially increase the number of crossovers used to form a mean height change. The above theories also predict that the standard errors of mean height changes from FHM will decrease or increase with increasing month, depending on the use of the upper or the lower parts of $\overline{\Delta \mathbf{H}'}$. However, for FFM the standard errors will be uniform through all months. With more crossovers used in FFM, the number of gaps in a height-change time series will be likely reduced. These advantages will be demonstrated in the special case in Sect. 2.2 and the numerical examples in Sect. 3. Note that, in the following development, the result from FHM is based on the computational formula in Eq. (9), which is currently used in the literature. [Eq. (12) is a new formula for FHM given in this paper.]

2.2 Comparison of ORM, FHM and FFM

Here we give a simplified, ideal case to show the advantage of FFM over ORM and FHM. Assume the standard error $\sigma_{i,j}$ and the number of crossovers $n_{i,j}$ to form the elements in $\overline{\Delta \mathbf{H}}$ for all bins are identical, that is, $n_{i,j} = n$, $\sigma_{i,j} = \sigma_0$ for all i, j. In this case, the standard errors and the numbers of crossovers are [see Eqs. (7), (10), (16) in this paper and Eqs. (6)–(7) in Ferguson et al. 2004]:

$$\begin{array}{lll} \bar{\sigma}_{1,j} = \sigma_0 & n_{1,j} = n, & \text{for ORM} \\ \bar{\sigma}_{i,j} = \begin{cases} \sigma_0, & i = 1 \\ \sqrt{2}\sigma_0, & i > 1, j > i \end{cases} & n_{i,j} = \begin{cases} n, & i = 1 \\ 2n, & i > 1, j > i, \end{cases} & \text{for FHM} \\ \bar{\sigma}_{i,j} = \begin{cases} \sigma_0, & i = 1 \\ \sqrt{2}\sigma_0, & i > 1, j \neq i \end{cases} & n_{i,j} = \begin{cases} n, & i = 1 \\ 2n, & i > 1, j \neq i, \end{cases} & \text{for FFM} \end{array} \tag{17}$$

with N months, the total numbers of crossovers are $n(N-1)$, $n(N-1)^2$ and $n(N-1)(2N-3)$ for ORM, FHM and FFM, respectively. Therefore, the total numbers of crossovers for FFM and FHM are $(2N-3)$ and $(N-1)$ times of that of ORM, respectively, and FFM almost doubles FHM ($(2N-3)$ vs. $(N-1)$) in the number of crossovers. The numbers of matrix elements for ORM, FHM and FFM are $(N-1)$, $(N-1)N/2$ and $(N-1)^2$, respectively. Hence, the numbers of matrix elements for FFM and FHM are $(N-1)$and $N/2$ times of that for ORM, respectively, and FFM doubles FHM in the number. The standard errors, $\bar{\sigma}_j$, and the total numbers of the height changes, n_j, for ORM, FHM and FFM are

$$\begin{array}{lll} \bar{\sigma}_j = \sigma_0 & n_j = n, & \text{for ORM} \\ \bar{\sigma}_j = \sigma_0\sqrt{4j-7}/(2j-3) & n_j = n(2j-3), & \text{for FHM} \\ \bar{\sigma}_j = \sigma_0\sqrt{4N-11}/(2\mathrm{N}-3) & n_j = n(2N-3), & \text{for FFM} \end{array} \tag{18}$$

Thus, for ORM and FFM, $\overline{\sigma}_j$ and n_j in $\overline{H}_j$ do not depend on j. Moreover, $\overline{\sigma}_j$ of FFM is $\sqrt{4N-7}/(2N-3)$ times of that of ORM, and n_j of FFM is $(2N-3)$ times that of ORM. Note that, for FHM, $\overline{\sigma}_j$ and n_j depend on j.

Figure 2 illustrates the differences in $\bar{\sigma}_j$ and n_j among ORM, FHM and FFM, using $\sigma_0 = 1$ cm, $N = 60$, $n = 9$. As predicted by the theory (see also Fig. 2a), n_j does not vary with j for both FFM and ORM. For FHM, n_j increases with j and falls between the numbers for ORM and FFM. For FHM, the average n_j in the first-half (FH) height-change time series ($j = 2, \ldots, 30$) is 261, which increases to 792 in the second-half (SH) ($j = 31, \ldots, 60$). For FHM, the

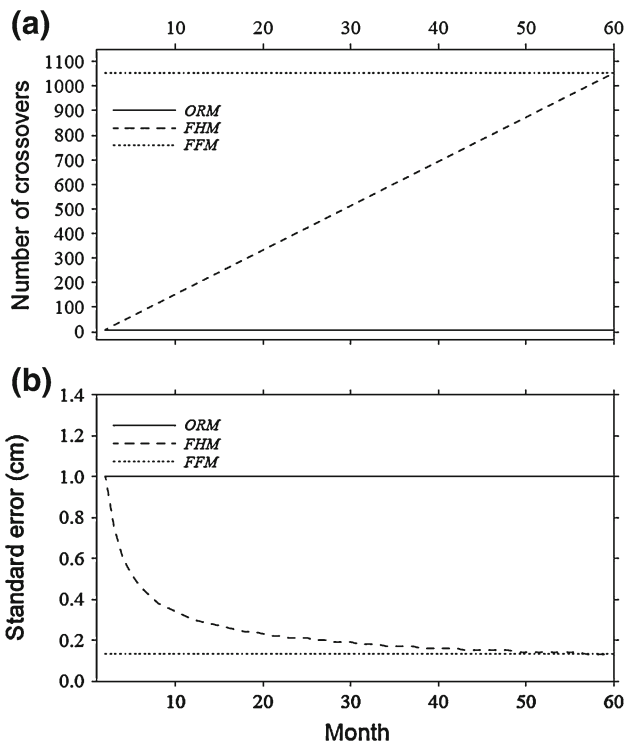

Fig. 2 Numbers of crossovers and standard errors for ORM, FHM and FFM using $\sigma_0 = 1$ cm, $N = 60$, $n = 9$

standard error decreases with increasing j, and this is also demonstrated in Fig. 3 of Ferguson et al. (2004). The non-uniform standard errors of FHM are shown in Fig. 2b: the means in the FH and SH time series are 0.32 and 0.15 cm, respectively. In contrast, the mean standard errors $\bar{\sigma}_j$ for all j are identical for FFM and ORM, and they are 0.13 and 1.0 cm, respectively. For FFM, n_j is much larger than that for ORM, and the former is 117 times of the latter (1,053 vs. 9). As a result, FFM leads to the least standard error (Fig. 2b). In summary, FFM achieves a uniform and the optimal precision throughout the entire height-change time series, which is not accomplished by the methods of ORM and FHM.

3 Numerical assessment of FFM using ENVISAT altimeter data

3.1 The ENVISAT altimeter data

For the numerical assessment and the case study in East Antarctica, we used altimeter data from the ENVISAT satellite mission. ENVISAT was launched in 2002 and was equipped with a satellite radar altimeter (RA2), a radiometer and a DORIS antenna. Ice sheet surface height measurements from the latest V2.1 Sensor Geophysical Data Record (SGDR) of ENVISAT altimeter were analyzed over the period from October 2002 to September 2007 in this paper. Compared to the data in the earlier versions, the data in V2.1 are corrected for the drift in the Ultra Stable Oscillator Clock (USO). Because the effect of terrain slope will be eliminated when forming the height difference at a crossover, we used ENIVSAT data without the slope correction. A consistent set of environmental, instrument corrections was applied to the ENVISAT altimeter data. However, the ocean tide corrections were not applied because our study area is on land. The surface heights in SGDR were derived from the ENVISAT altimeter range measurements, which were corrected by the waveform effect using the ICE-2 algorithm of waveform retracking (Legresy et al. 2005). In this paper, we derived height changes from ENVISAT at 1-month interval (they are called monthly height changes below). As an example, Fig. 3 shows the ENVISAT data distribution in July 2003.

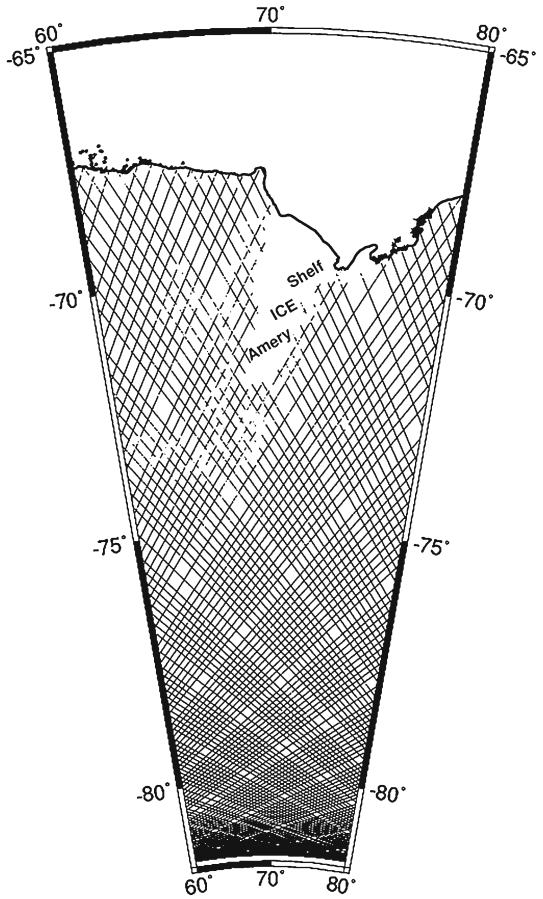

Fig. 3 The distribution of ENVISAT ground tracks in July 2003 in the study area

3.2 Assessment of height change determination by FFM

In this section, the numerical assessment focuses on the five issues: (1) the number of crossovers, (2) the elements of matrices containing height changes, (3) the number of months in $\overline{H}_j$, $j = 2, \ldots, N$, (4) the mean value of $\bar{\sigma}_j$'s of $\overline{H}_j$, and (5) the mean value of $\bar{\sigma}_j$'s of $\overline{H}_j$ in the FH and SH of the monthly height-change time series from ENVISAT. For the assessment, we determined the height changes for all $2^\circ \times 1^\circ$ bins in the study area (Fig. 1) and discarded the bins satisfying any of the following three criteria (Li and Davis 2006): (1) a bin with less than 5,000 crossovers, (2) a bin resulting in less than 20 % of the maximum number of elements (i.e., about $0.2 \times (N-1)^2$) in $\overline{\Delta \mathbf{H}'}$, and (3) a bin containing less than 20 % of the data months (i.e., $0.2 \times (N-1)$).

As an example, Fig. 4 shows the monthly height changes from three methods over the $2^\circ \times 1^\circ$ bin centered at 70.5°S, 65°E. The monthly height changes from the lower triangular matrix of Eq. (12), denoted as FHM_L, are also shown in Fig. 4c. All height changes from the three methods show a strong seasonal variation, with a peak value up to 50 cm. Starting from the 16th month (corresponding to February 2004), there is a positive linear trend (the dashed lines in Fig. 4) in the height changes from all methods. There are many data gaps in the ORM-derived height changes (16 months missing), and the standard errors of such height changes are relatively large compared to those from the other two methods (Fig. 4b, d). The result from FHM contains less data gaps (missing data in the 2nd, 5th and 51st months) and the overall standard errors are less than those

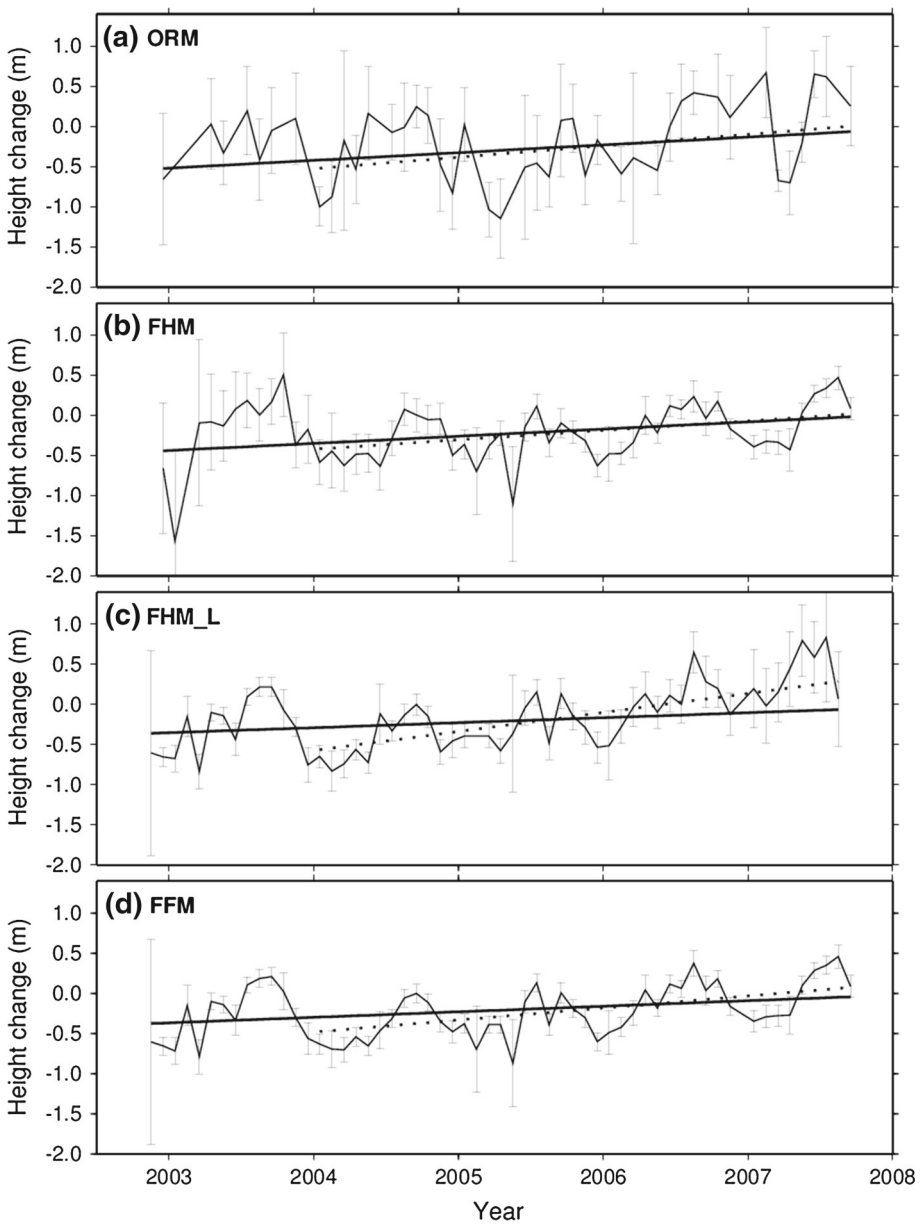

Fig. 4 Monthly height changes from ENVISAT with one-sigma error bars, starting from October 2002, at the $2^\circ \times 1^\circ$ bin centered at 70.5° *S*, 65°E, from ORM, FHM, FHM_L (based on Eq. (12)) and FFM. The linear trends starting from October 2002 (*solid lines*) and from February 2004 (*dashed lines*) are also plotted

from ORM. As the theory [Eqs. (8) and (12)] predicts, the standard error of height change from the upper/lower triangular matrix (FHM_L) decreases/increases with time (Fig. 4b, c). There is only one data gap (in the 51st month, corresponding to January 2007) from FFM (Fig. 4c). Using the weighted least-squares method, we estimated the linear height rates of the four time series (ORM, FHM, FHM_L and FFM) in Fig. 4a–d, which are 9.61 ± 0.24, 8.92 ± 0.56, 6.22 ± 0.50 and 6.88 ± 0.02 cm/year, respectively. Because of the non-uniform errors in the heights, the standard errors of the rates for FHM and FHM_L are relatively large and but are close (0.56 and 0.50 cm/year). The standard error of the rate for FFM is the least, showing the effectiveness of FFM in reducing the error in the estimated rate. This suggests that the additional observations used in FFM improve the overall quality in the ENVISAT height changes: FFM produces height changes with the smallest and the most uniform standard errors throughout the entire height-change time series. The FFM result also shows the most pronounced seasonal variation in height, compared to the results from ORM and FHM.

Table 1 summarizes the results of the height changes from three methods over the bin at 70.5°S, 65°E. The number of crossovers from FFM is about 23,794, which is 1.9 and 79 times more than the numbers from FHM and ORM, respectively. The number of elements in $\overline{\Delta \mathbf{H}'}$ from FFM is two times more than that from FHM. The mean standard error of height changes is about 48 cm for ORM, reduced to 28 cm by FHM, and to 17 cm by FFM. For FHM, the overall precision

of the SH height-change times series is better than that of the FH height-change time series (18 vs. 39 cm); this result is due to the different numbers of height changes used to form the FH and SH time series [Eq. (7) in Ferguson et al. (2004)]. Both ORM and FFM achieve a nearly uniform height error over the FH and SH height-change time series, but the overall height error from FFM is much smaller than others because FFM uses much larger numbers of observations.

A further comparison of the accuracies of height changes from the three methods was made over the entire study area. We assessed the results in two sub-areas according to latitude: Area 1 (lower latitude) is over 68°−75°S, and Area 2 (higher latitude) is over 75−81.6°S. The statistics for Areas 1 and 2, and the entire area are summarized in Table 2. In the three areas, FFM always produces more crossovers than the other two methods. For example, the mean number of crossovers from FFM is about 2 and 118 times more than those from FHM and ORM, respectively. As for the matrix elements, FFM is about two times more than FHM. Both the number of crossovers and height precision increase with absolute latitude. For example, ORM results in a mean latitude error of 6 cm in Area 2, which is just about 1/4 that of Area 1 (24 cm). Although FHM can improve the height precision over ORM, FHM results in non-uniform accuracies in the FH and SH height-change time series. For example, in Area 1, FHM delivers a mean error of 12 cm in the FH time series, compared to 6 cm in the SH time series. This drawback of FHM has been pointed out in the example associated with Table 1. FFM can both improve the height precision over FHM and ORM and maintain a uniform precision in the entire time series. For example, FFM results in mean errors of 5 and 1 cm in Areas 1 and 2, respectively, in both halves of the time series. The result from Table 2 indicates that the height precision increases with absolute latitude for all methods, and FFM delivers the least height errors.

In summary, the numerical result in this section is consistent with the predicted result in Sect. 2.1. That is, FFM achieves (1) the maximum number of crossovers, (2) the least data gaps in the full time series of height change, and (3) uniform and least standard errors in the time series.

Table 1 Statistics of the results from three methods over the 2° × 1° bin centered at 70.5°S, 65°E

Method	A	B	C	D	E	F
ORM	300	43	43	0.50	0.47	0.48
FHM	12,273	846	56	0.39	0.18	0.28
FFM	23,794	1,694	58	0.20	0.15	0.17

A no. of crossovers, *B* no. of matrix elements, *C* no. of monthly values in the height-change time series, *D* mean standard error in the first-half (FH) time series (m), *E* mean standard error in the second-half (SH) time series (m), *F* mean standard error in the time series (m)

4 Result of ice sheet height change from ENVISAT using FFM

4.1 Improved correlation between height change and backscattered power change by FFM

In Sect. 3.2, we have computed the monthly height-change time series by FFM for all 2° × 1° bins in the study area using the ENVISAT altimeter data. Here, we discuss the backscatter effect on height changes. The backscatter effect is a function of the surface and/or sub-surface scattering characteristics of the ice sheet. Different altimeters, retracking

Table 2 Statistics of the results from three methods over three latitude-averaged areas (definitions of D–F are the same as those given in Table 1)

Method	A1	B1	C1	D	E	F
(a) Area 1: latitude 68°−75°S, longitude 60°−80°E						
ORM	868.04	56.91	56.91	0.24	0.24	0.24
FHM	50, 402.93	1, 606.31	58.63	0.12	0.06	0.09
FFM	99, 924.80	3, 214.26	58.82	0.05	0.05	0.05
(b) Area 2: latitude 75°−81.6°S, longitude 60°−80°E						
ORM	3, 793.97	59	59	0.06	0.06	0.06
FHM	227, 186.83	1, 711	59	0.03	0.01	0.02
FFM	451, 103.91	3, 422	59	0.01	0.01	0.01
(c) Entire area: latitude 68°−81.6°S, longitude 60°−80°E						
ORM	2, 506.56	58.08	58.08	0.14	0.14	0.14
FHM	149, 401.91	1, 664.94	58.84	0.07	0.03	0.05
FFM	296, 585.10	3, 330.59	58.92	0.03	0.03	0.03

A1 mean no. of crossovers, *B1* mean no. of matrix elements, *C1* mean no. of monthly values in the height-change time series

algorithms, and locations of analysis will result in different backscatter effects. Wingham et al. (1998, using ORM) and Davis and Ferguson (2004, using FHM) showed that backscattered power change of a radar altimeter can result in false height change. For most of the $2^\circ \times 1^\circ$ bins in Antarctica (defined in the same manner as in this paper; see Sect. 2.1), Wingham et al. (1998) found that the correlation coefficients between changes in height and in backscattered power exceed 0.7. Davis and Ferguson (2004) found only 50 % of the $2^\circ \times 1^\circ$ bins in their study area having correlation coefficients over 0.7. In addition, Zwally et al. (2005) and Yi et al. (2001) discussed several criteria when applying backscatter corrections to altimeter-derived height changes. Khvorostovsky and Johannessen (2009) showed that the correlation coefficient varies with time. When deriving the correlation coefficients in the paper, the height and backscattered power changes were the weighted means as computed by Eq. (14).

Table 3 Statistics of the correlation coefficients between height-change rates (cm/year) and backscattered power change from ORM, FHM and FFM over 60°−79°S, 60°−74°E

Method	Max	Min	Mean	SD
ORM	0.96	−0.17	0.70	0.26
FHM	0.98	−0.11	0.82	0.20
FFM	0.98	−0.04	0.85	0.17

To stress the importance of improved height precision for an improved estimation of backscatter effect, we computed the backscatter–height correlation coefficients using heights determined by ORM, FHM and FFM over the entire study area (Fig. 1). For each bin, we then determined the correlation coefficient $\bar{R}$ between the height and the backscatter time series. Table 3 shows the statistics of the backscatter–height correlation coefficients from all bins using the heights and backscatters from ORM, FHM and FFM. The maximum correlation coefficient increases from 0.96 (ORM) to 0.98 (FHM and FFM). The mean correlation coefficients for ORM, FHM and FFM are 0.70, 0.82 and 0.85, respectively, with the standard deviations of correlation coefficients being 0.26, 0.20 and 0.17, respectively. Hence, FFM increases the overall correlation between backscatter and height change, which in turn yields a better estimate of backscatter effect for height correction.

As an example, Fig. 5 compares the monthly height changes (from FFM) and backscattered power changes at the $2^\circ \times 1^\circ$ bins centered at 80.5°S, 65°E (the interior bin) and at 70.5°S, 65°E (the coastal bin). At the interior bin (Fig. 5a), the uncorrected height changes (the method of backscatter correction is shown in Sect. 4.2 below) are strongly correlated with the backscattered power changes, with a

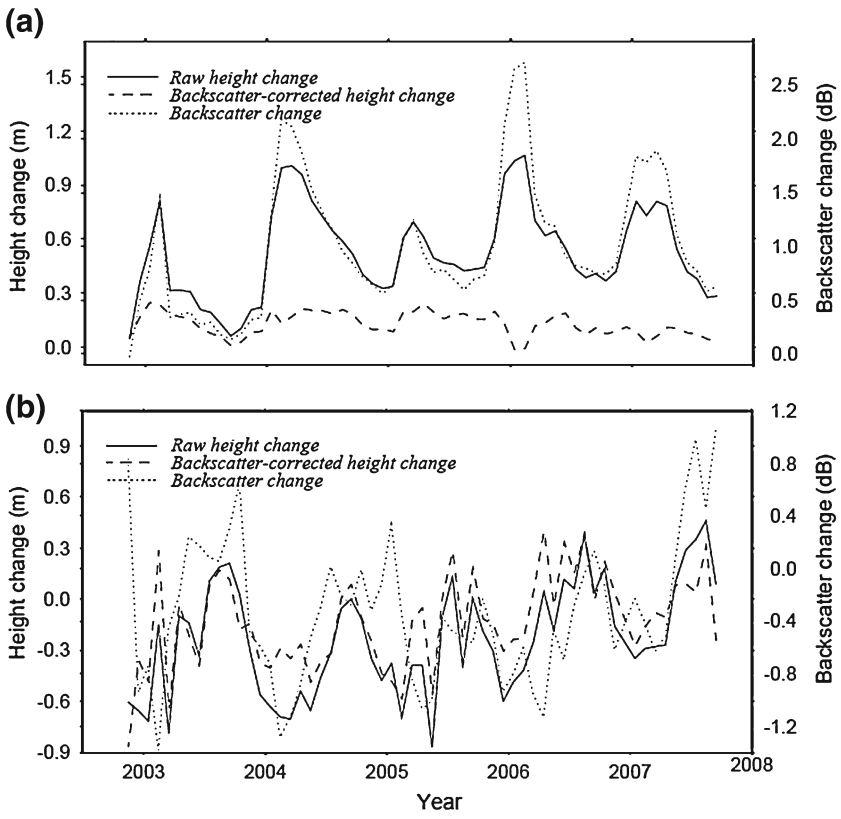

Fig. 5 Monthly backscattered power changes and height changes (corrected and uncorrected) at the $2^\circ \times 1^\circ$ bins centered at **a** 80.5°S, 65°E and **b** 70.5°S, 65°E

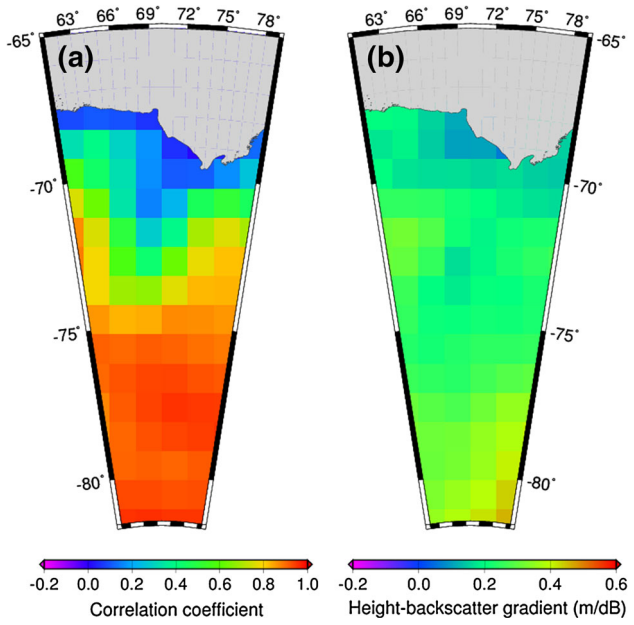

Fig. 6 Spatial distributions of **a** height–backscatter correlation coefficients $\bar{R}$ and **b** height–backscatter gradient

correlation coefficient of 0.97. At the annual and interannual time scales, the height changes are coherent with the backscattered power changes. In addition, the maximum peak-to-trough seasonal height change reaches 1 m, which is too large for an interior bin in East Antarctica, where the annual snow accumulation is roughly 12 cm/year (Vaughan et al. 1999). In contrast, the coastal bin (Fig. 5b) shows a moderate height–backscatter correlation coefficient of 0.53. Like the interior bin, the seasonal variation and the height-change rate at the coastal bin are affected by backscattered power change, but only to a limited extent.

Figure 6a shows the distribution of the height–backscatter correlation coefficients for all $2° \times 1°$ bins (the heights are from FFM). The correlation coefficients tend to be higher in the interior of East Antarctica and smaller near the coasts. The correlation coefficients over the Amery Ice Shelf are mostly less than 0.4 and are smaller than the coefficients elsewhere. On the Amery Ice Shelf, the mean and standard deviation (SD) of the correlation coefficients are 0.30 and 0.13, respectively, while they are about 0.87 and 0.15 elsewhere. Excluding the bins near the coasts and the Amery Ice Shelf, the mean and SD of the correlation coefficients are 0.91 and 0.06, respectively. The accuracies of height change from ENVISAT over the Amery Ice Shelf and the coastal zone may be affected by ocean tide variations, as we did not apply tidal corrections to the ENIVSAT data used in this paper. Tidal correction may increase the correlations between height changes and backscattered power changes here.

4.2 Backscatter effect on ENVISAT-derived height

The results from Sect. 4.1 show that the raw ENVISAT-derived height changes are highly correlated with the backscattered power changes over most part of the study area. Using the correlation coefficients given in Fig. 6a, the raw height changes were corrected for the backscatter effect as follows. The backscatter correction, $\overline{H}_{S(j)}$, was computed for each month as the negative product of the height–backscatter gradient h_{B} and $\overline{\sigma_0}_j$ (Davis and Ferguson 2004):

$$\overline{H}_{S(j)} = -\overline{\sigma_0}_j \cdot h_{\mathrm{B}} \tag{19}$$

where h_{B} is the height–backscatter gradient and the negative sign indicates that a positive backscattered power change can induce a negative height change. In this paper, the height–backscatter gradient at a bin was computed as the ratio between height change and backscattered power change from the height and backscatter time series (see Eq. (1) in Davis and Ferguson 2004). The distribution of the height–backscatter gradients in the study area is shown in Fig. 6b. The color scales and quantities in Fig. 6a and b are different (correlation coefficient vs. height–backscatter gradient), but there is a high degree of similarity between the two plots. For example, in the coast, both the correlation coefficient and gradient are low, suggesting large height uncertainties here. At higher latitudes (south of $-75°$), both two quantities are simultaneously larger and this is the result of (1) more crossovers in the interior of Antarctica, and (2) improved height precision by FFM. In general, height–backscatter gradient increases with height–backscatter correlation coefficient. The height–backscatter gradients over the Amery Ice Shelf and the coasts are less than 0.15 m/dB and are smaller than the values elsewhere. The mean and SD values of the height–backscatter gradients over the Amery Ice Shelf and coasts are 0.14 and 0.09 m/dB, respectively, compared to 0.30 and 0.10 m/dB elsewhere. This result is consistent with that of Davis and Ferguson (2004).

Again, we used the two sample bins in Fig. 5 to examine the backscatter effect on height change. For each of the two bins, we computed the amplitude of the seasonal variation and the height-change rate with and without backscatter correction. As stated before, at the interior bin (Fig. 5a), the raw height changes contain large annual variations. After the backscatter correction, the annual height variations become reasonable: the mean seasonal amplitude is reduced to 0.03 from 0.23 m, and the height-change rate is reduced to -0.01 from 0.05 m/year. The changes in amplitude and rate are also seen at the coastal bin (Fig. 5b): the mean seasonal amplitude changes from 0.27 to 0.12 m, and the rate from 0.06 to 0.05 m/year. The two examples in Fig. 5 highlight the fact that the backscatter correction will significantly alter the result of a height-change time series derived from ENVISAT.

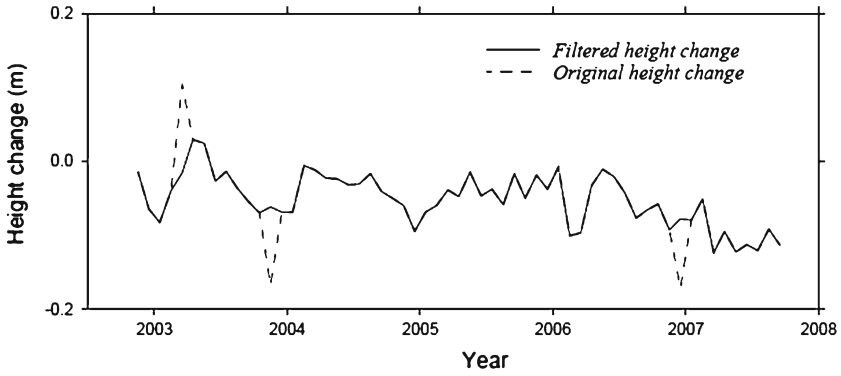

Fig. 7 Filtered and original monthly height changes at the $2^\circ \times 1^\circ$ bin centered at 78.5°S, 63°E, with three outliers removed from the original heights

Such an alteration is consistent with that reported by Davis and Ferguson (2004).

4.3 Height-change rate over the ice sheet of East Antarctica

4.3.1 Filtering raw height change and removing outlier

Before computing the height-change rate, we applied filtering to raw height changes as follows. A filtered height change was obtained by convolving the raw height changes with the time-dependent Gaussian function (Hwang and Hsu 2008)

$$g(\Delta t) = \mathrm{e}^{-\frac{\Delta t^2}{\sigma^2}} \tag{20}$$

where σ is the 1/6 of the given window size (in time) of convolution, Δt is the time difference between the targeted month (the month where a smoothed height change is desired) and the running month. An iterative process was used to remove outliers in height changes while filtering height changes. First, the differences between the raw and filtered heights were computed for all months, and the SD of the differences was found. The largest difference that exceeds three times of the SD was considered as an outlier and the corresponding height change was removed. This process was repeated without the removed height. The iteration stops when no outlier was found. The data gaps (due to removed outliers) were filled using values interpolated from the outlier-free data. As shown in Sect. 3, the SDs of height changes from FFM are quite uniform throughout the entire height-change time series. As an example, Fig. 7 shows the raw and filtered height changes over the bin centered at 78.5°S, 63°E. In this example, the iterative process has removed three outliers. Except at the months with outliers, the filtered and the original height-change time series do not differ significantly from each other, because the former was derived by averaging the height changes over the bin (for a given month).

4.3.2 The best threshold correlation coefficient (TCC) for ENVISAT using the ICESat result

Figure 6 suggests that the degree of correlation between height and backscatter can vary from one bin to another in the study area. If the height–backscatter correlation coefficient is low, applying the backscatter correction will result in an extra error in the original (raw) height (Zwally et al. 2005); see also Sect. 4.1. Therefore, we applied the backscatter correction to a raw height at a given bin only when the height–backscatter correlation coefficient here exceeds a given threshold correlation coefficient (TCC), based on Zwally et al. (2005). That is, a backscatter-corrected height change is computed as

$$\overline{H}_{R(j)} = \overline{H}_j - f \cdot \overline{\sigma_0}_j \cdot h_\mathrm{B} \tag{21}$$

where f is defined as

$$f = \begin{cases} 0, & \text{if } \bar{R} < R_T \\ 1, & \text{if } \bar{R} \geq R_T \end{cases} \tag{22}$$

with $\bar{R}$ and R_T being correlation coefficient and TCC, respectively. Note that, we did not consider TCC in the case study of Fig. 5, i.e., $f = 1$. It turns out the selection of the best TCC is difficult. After several attempts, we decide to determine the best TCC using the height-change rates of ICESat. The ICESat result we used is from Yamamoto et al. (2008), who used ICESat data over October 2003 to April 2007 in the area over 65°−79°S and 61°−73°E. The uncertainty of a single height measurement of ICESat is about 10 cm. According to Schutz et al. (2005), ICESat can determine height-change rates over polar ice sheets to better than 1 cm/year and does not have the problem of backscatter effect. For the best TCC determination, the height-change rates from ENVISAT were computed for all bins over the same time span and area as for the ICESat result of Yamamoto et al. (2008). According to the result of the inter-campaign comparison of Gunter et al. (2009), we removed a bias of 2.3 cm/year from the ICESat rates of Yamamoto et al. (2008) for all bins.

We experimented with $-0.2 \leq \mathrm{TCC} \leq 1.1$ at an interval of 0.01 to see the relationship between TCC and standard deviation of height differences (ENVISAT vs. ICESat), and

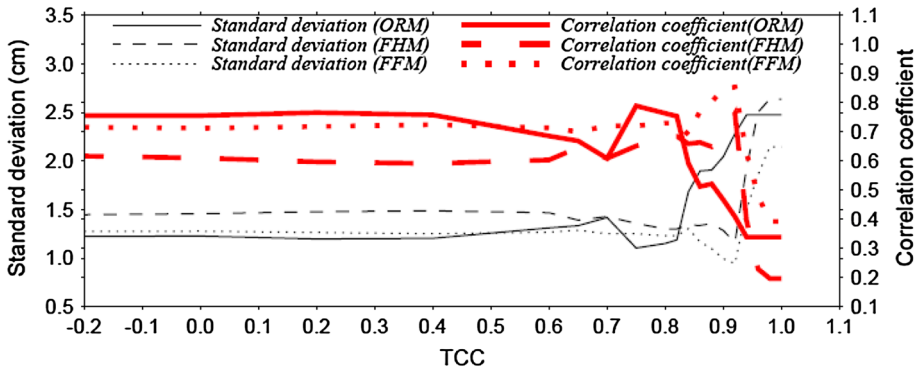

Fig. 8 Correlation coefficients between height changes from ICESat and from ENVISAT (by ORM, FHM and FFM), and the standard deviations of height differences (ICESat vs. ENVISAT)

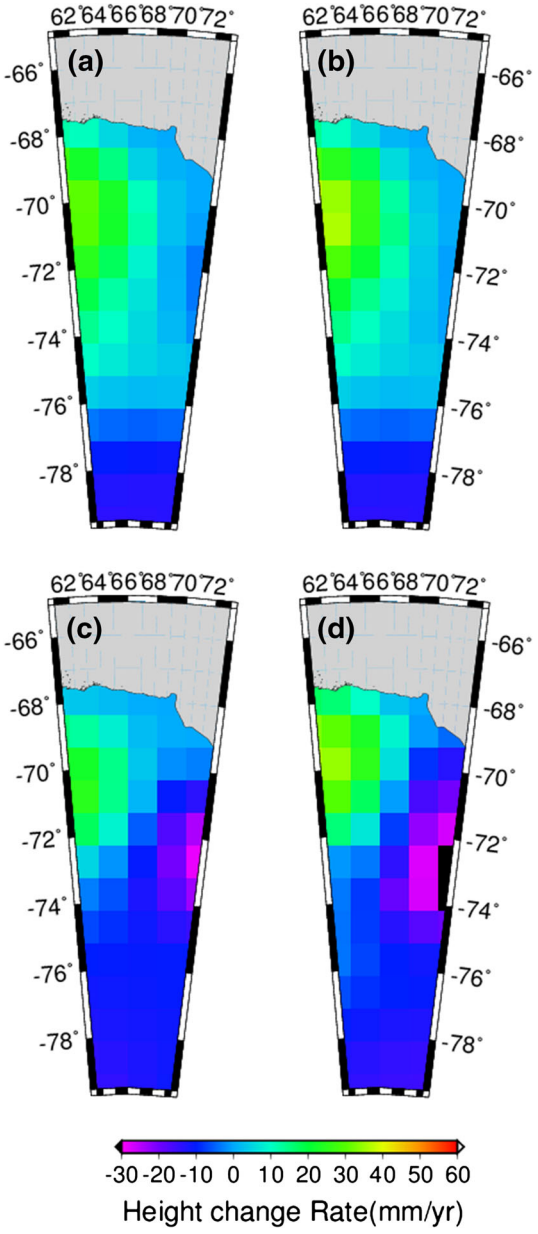

Fig. 9 Spatial distributions of height-change rates from **a** ENVISAT with $R_T = 0.5$, **b** ENVISAT with $R_T = 0.7$, **c** ENVISAT with $R_T = 0.9$, **d** ICESat

Table 4 Statistics of the differences between height-change rates (cm/year) from ICESat and ENVISAT based on three threshold correlation coefficients (TCCs) over 60°−79°S, 60°−74°E

TCC	Max	Min	Mean	SD
0.5	5.13	−1.47	0.93	1.26
0.7	5.13	−1.47	0.83	1.25
0.9	4.43	−2.22	0.03	0.99

the relationship between TCC and height–backscatter correlation. Figure 8 shows the result: TCC = 0.92 leads to the highest correlation of 0.85 (height changes from FFM) and a standard deviation of 0.94 cm. We also determined the optimal TCC values from the height changes from ORM and FHM, as shown in Fig. 8. The optimal TCC for FHM is also 0.92, leading to the maximum correlation coefficient of 0.76 and the minimum standard error of 1.16 cm. For ORM, the optimal TCC is 0.75, which results in the maximum correlation coefficient of 0.79 and the minimum standard error of 1.10 cm. In comparison to ORM and FHM, FFM increases the height–backscatter correlation and reduces the standard deviation of height differences.

To demonstrate the impact of TCC on the ENVISAT-derived height-change rates, Fig. 9a–c shows the height-change rates from ENVISAT using TCC = 0.5, 0.7 and 0.9, and Fig. 9d shows the rates from ICESat. Table 4 shows the statistics of the differences between the height changes from ICESat and from ENVISAT based on the three TCCs. The mean of the ICESat–ENVISAT differences in the case of TCC = 0.5 differs by 0.1 cm/year from the mean in the case TCC = 0.7. The standard deviations of the differences in the two cases differ by 0.01 cm/year. However, there is a sharp difference between the cases of TCC = 0.5 and TCC = 0.9: the mean and standard deviation of the ICESat–ENVISAT height differences are reduced to 0.03 and 0.99 cm/year from 0.93 and 1.26 cm/year, respectively. With TCC = 0.9, we obtained the highest correlation coefficient of 0.85 between the height changes from ICESat and ENVISAT in the study area. This suggests that the backscatter correction for ENIVISAT by Eq. (20) can be made more accurate

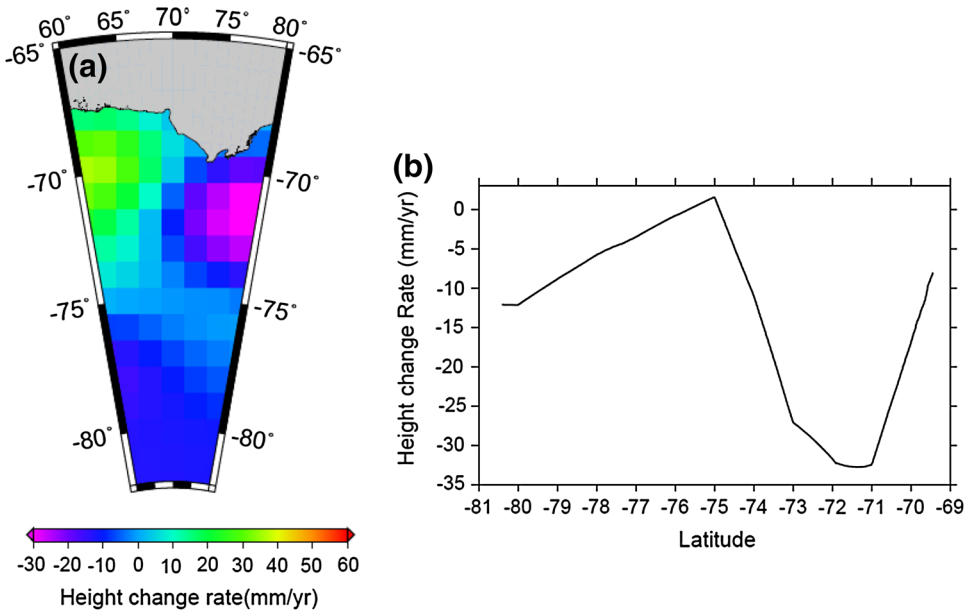

Fig. 10 ENVISAT-derived height-change rates (with backscatter correction) over October 2002 to September 2007, **a** in the study area **b** along the CHINARE route as a function of latitude

(in terms of the agreement with the ICESat result) when the height–backscatter correlation coefficient exceeds 0.9.

4.3.3 ENVISAT-derived height-change rates in East Antarctica and along CHINARE

Using the best TCC, i.e., $R_T = 0.92$, we determined the height-change rates from ENVISAT in the study area over October 2002 to September 2007 (Fig. 10a). Figure 10b shows the height-change rates along the CHINARE route. The height-change rates (Fig. 10a) are not spatially uniform in the study area and mostly fall between −3 and 3 cm/year. West of the Amery Ice Shelf and in the latitude range of 68−75°S, the rates are mostly positive with a peak value of 3 cm/year. East of the Amery Ice Shelf, the rates are mostly negative. Along the CHINARE route (Figs. 1, 10b), the rate near Zhongshan Station is about −1 cm/year, and it (absolute value) increases with latitude, reaching about −3 cm/year between 71−72°S. South of 72°S, the rate starts to decrease, reaching almost zero at 75°S. South of this point, again the rate (absolute value) increases with latitude, finally reaching about −1 cm/year at the finishing point near Kunlun Station. A future work will be to compare this spatial pattern of height-change rate with the spatial patterns of surface mass balance (Ding et al. 2011) and horizontal velocity (Zhang et al. 2008) along CHINARE, to cross-validate the remote sensing result (this paper) and the ground measurement result.

5 Conclusions

We demonstrate the theory and numerical results of FFM. FFM forms a full matrix referring to the first month using the modified relationship among the elements in the upper triangular matrix of FHM. Using the ENVISAT altimeter data, we show that FFM results in a substantial increase in the numbers of crossovers and matrix elements, compared to such numbers from FHM and ORM. The mean standard errors of height change from FFM are significantly smaller than those from FHM and ORM. The mean latitude error from FFM is about 1/2 and 1/5 of those from FHM and ORM, and it increases with absolute latitude. FFM can improve not only the height precision, but also maintain a uniform precision in the entire height-change time series (FHM loses precision in the FH height-change time series).

We also investigate the backscatter effect on ENVISAT-derived height changes. In general, the height–backscatter correlation is low near the coast of East Antarctica and Amery Ice Shelf (about 0.3 on average) and is high in the interior of East Antarctica (about 0.9 on average). The ICESat height-change rates are used to assist the determination of the best TCC for the backscatter correction for ENVISAT, which is 0.9 among three tested TCC values. The ENVISAT-derived height-change rates mostly fall between −3 and 3 cm/year, with a large spatial variability in East Antarctica. We believe that the ENVISA-derived height-change rates along CHINARE (Fig. 10b) will serve as a constraint for the ground-based mass balance result, which is derived from only snow-stick and GPS measurements from Zhongshan Station to Kunlun Station.

A satellite-derived height-change field like the one given in Fig. 10a can be used to plan an optimal route for future fieldwork to collect data at key spots for mass balance studies and to improve the glacier-isostatic adjustment model in Antarctica. In principle, the method of FFM and the method of backscatter analysis in this paper are also applicable to

detection of height change using properly retracked altimeter on a land mass that is not covered by ice, such as Tibetan Plateau. This is a subject for future studies.

Acknowledgments We thank the European Space Agency for providing the ENVISAT SGDR data through the AVISO CNES Data Center. This study is supported by the MOST (Grant No. 2013CBA01804), National Natural Science Foundation of China (Grant No. 41106163, No. 41128003 and No. 41076126), and SOA (Grant No. CHINARE 2013, 2014). We thank the three reviewers, who provide very constructive comments that greatly improve the quality of this paper.

References

Church JA, Gregory JM, Huybrechts P, Kuhn M, Lambeck K, Nhuan MT, Qin D, Woodworth PL (2001) Changes in sea level. In: Houghton JT (ed) Climate change 2001: the scientific basis. Contribution of working group I to the third assessment report of the intergovernmental panel on climate change. Cambridge University Press, Cambridge, pp 639–694

Davis CH, Segura DM (2001) An algorithm for time-series analysis of ice sheet surface elevations from satellite altimetry. IEEE Trans Geosci Remote Sens 39:202–206

Davis CH, Ferguson AC (2004) Elevation change of the Antarctic ice sheet, 1995–2000, from ERS-2 satellite radar altimetry. IEEE Trans Geosci Remote Sens 42:2437–2445

Ding M, Xiao C, Li Y, Ren J, Hou S, Jin B, Sun B (2011) Spatial variability of surface mass balance along a traverse route from Zhongshan station to Dome A, Antarctica. J Glacio 157(204):658–666

Ferguson AC, Davis CH, Cavanaugh JE (2004) An autoregressive model for analysis of ice sheet elevation change time series. IEEE Trans Geosci Remote Sens 42:2426–2436

Fu LL, Cazenave A (2001) Satellite altimetry and earth sciences: a handbook of techniques and applications. Academic, San Diego

Gunter B, Urban T, Riva R, Helsen M, Harpold R, Poole S, Nagel P, Schutz B, Tapley B (2009) A comparison of coincident GRACE and ICESat data over Antarctica. J Geod 83:1051–1060

Hwang C, Hsu HY (2008) Shallow-water gravity anomalies from satellite altimetry: case studies in the East China Sea and Taiwan Strait. J Chin Inst Eng 31(5):841–851

Khvorostovsky K, Johannessen OM (2009) Merging of ERS-1, ERS-2 and Envisat altimeter data over the Greenland ice sheet. Nansen Environ Remote Sens Center, Bergen, Norway, Technical Report 307

Legresy B, Papa F, Remy F, Vinay G, Bosch M, Zanife OZ (2005) ENVISAT radar altimeter measurements over continental surfaces and ice caps using the ICE-2 retracking algorithm. Remote Sens Environ 95:150–163

Li Y, Davis CH (2006) Improved methods for analysis of decadal elevation-change time series over Antarctica. IEEE Trans Geosci Remote Sens 44:2687–2697

Rémy F, Parouty S (2009) Antarctic ice sheet and radar altimetry: a review. Remote Sens 1:1212–1239

Schutz BE, Zwally HJ, Shuman CA, Hancock D, DiMarzio JP (2005) Overview of the ICESat mission. Geophys Res Lett 32(21). doi:10.1029/2005GL024009

Tapley BD, Bettadpur S, Ries JC, Thompson PF, Watkins M (2004) GRACE measurements of mass variability in the earth system. Science 305(5683):503–505

Vaughan DG, Bamber JL, Giovineto M, Russell J, Cooper APR (1999) Reassessment of net surface mass balance in Antarctica. J Clim 12:933–946

Velicogna I, Wahr J (2006) Measurements of time-variable gravity show mass loss in Antarctica. Science 311(5768):1754–1756. doi:10.1126/science.11237785

Wahr J, Wingham D, Bentley C (2000) A method of combining ICESat and GRACE satellite data to constrain Antarctic mass balance. J Geophys Res 105(B7):16279–16294

Wingham DJ, Ridout AJ, Scharroo R, Arthern RJ, Ck Shum (1998) Antarctic elevation change from 1992 to 1996. Science 282:456–458

Wingham DJ, Shepherd A, Muir A, Marshall GJ (2006) Mass balance of the Antarctic ice sheet. Philos Trans R Soc A 364(1844):1627–1635

Yamamoto K Fukuda Y, Doi K, Motoyama H (2008) Interpretation of the GRACE-derived mass trend in Enderby Land, Antarctica. Polar Sci 2(4):267–276

Yi D, Bentley CR, Stenoien MD (1997) Seasonal variation in the apparent height of the East Antarctic ice sheet. Ann Glaciol 24:191–198

Yi D, Zwally HJ, Cornejo HG, Barbieri K, DiMarzio J (2001) Elevations observed by satellite radar altimeter over ice sheets to variations in backscatter power and derived corrections. CryoSat Validation Workshop 2011, Frascati, Italy, February 2001

Zhang S, E D, Wang Z, Li Y, Jin B, Zhou C (2008) Ice velocity from static GPS observations along the transect from Zhongshan station to Dome A, East Antarctica. Ann Glaciol 48:113–118

Zwally HJ, Brenner AC (2001) Ice sheet dynamics and mass balance. In: Fu LL, Cazenave A (eds) Satellite altimetry and earth sciences: a handbook of techniques and applications. Academic Press, Orlando, pp 351–369

Zwally HJ, Brenner AC, Major JA, Bindschadler RA, Marsh JG (1989) Growth of Greenland ice sheet: measurement. Science 246:1587–1589

Zwally HJ, Giovinetto MB, Li J, Cornejo HG, Beckley MA, Brenner AC, Saba JL, Yi D (2005) Mass changes of the Greenland and Antarctic ice sheets and shelves and contributions to sea-level rise: 1992–2002. J Glaciol 51(175):509–527